Eur. J. Mineral., 37, 39–52, 2025
https://doi.org/10.5194/ejm-37-39-2025

European Journal of Mineralogy
Open Access

Dacostaite, $K(Mg_2Al)[Mg(H_2O)_6]_2(AsO_4)_2F_6 \cdot 2H_2O$, a new fluoride–arsenate mineral from the Cetine di Cotorniano Mine (Tuscany, Italy)

Cristian Biagioni[1,2], Daniela Mauro[1,3], Jiří Sejkora[4], Zdeněk Dolníček[4], Andrea Dini[5], and Radek Škoda[6]

[1]Dipartimento di Scienze della Terra, Università di Pisa, Via Santa Maria 53, 56126 Pisa, Italy
[2]Centro per l'Integrazione della Strumentazione scientifica dell'Università di Pisa (CISUP), Università di Pisa, Pisa, Italy
[3]Museo di Storia Naturale, Università di Pisa, Via Roma 79, 56011 Calci, Italy
[4]Department of Mineralogy and Petrology, National Museum, Cirkusová 1740, 193 00 Prague, Czech Republic
[5]Istituto di Geoscienze e Georisorse, Consiglio Nazionale delle Ricerche, Via Moruzzi 1, 56124 Pisa, Italy
[6]Department of Geological Sciences, Faculty of Science, Masaryk University, Kotlářská 2, 611 37 Brno, Czech Republic

Correspondence: Cristian Biagioni (cristian.biagioni@unipi.it)

Received: 6 October 2024 – Revised: 22 November 2024 – Accepted: 25 November 2024 – Published: 20 January 2025

Abstract. The new mineral dacostaite, $K(Mg_2Al)[Mg(H_2O)_6]_2(AsO_4)_2F_6 \cdot 2H_2O$, has been discovered in the Cetine di Cotorniano Mine, Chiusdino, Siena, Tuscany, Italy. It occurs as thin, colourless-to-white pseudo-hexagonal micaceous crystals up to 0.5 mm in size. The streak is white, and the lustre is silky. The cleavage is perfect on {001}. The empirical formula of dacostaite, based on (As + P) = 2 atoms per formula unit, is $(K_{0.56}Ca_{0.04}Na_{0.03}\square_{0.37})_{\Sigma 1.00}$ $(Al_{1.54}Mg_{1.38}Cu_{0.03}Zn_{0.03})_{\Sigma 2.98}$ $[Mg(H_2O)_6]_2$ $[(As_{0.99}P_{0.01})O_4]_2$ $[F_{4.46}(OH)_{1.46}O_{0.08}]_{\Sigma 6.00} \cdot 2H_2O$ ($Z = 2$). Dacostaite is monoclinic, with a space group of $C2/m$ and $a =$ 12.474(5), $b = 7.198(3)$, $c = 13.724(6)$ Å, $\beta = 99.518(13)°$, and $V = 1215.3(8)$ Å^3. The crystal structure was solved using single-crystal X-ray diffraction data and refined to $R_1 = 0.0927$ for 1022 unique reflections with $F_o > 4\sigma$ (F_o). The crystal structure of dacostaite can be described as formed by heteropolyhedral {001} layers and isolated $Mg(H_2O)_6$ groups connected by H bonds. In the type material, dacostaite is associated with quartz, sulfur, gypsum, and a pharmacosiderite-like mineral in a small cavity of silicified limestone. Its genesis is related to the activity of oxidized (Al,F)-rich fluids during the late-stage evolution of the Sb ore deposit formerly exploited at the Cetine di Cotorniano Mine.

1 Introduction

In the second half of the 1940s, Fornaseri (1947) described the occurrence of an Sb oxychloride at the Cetine di Cotorniano Mine (Tuscany, Italy), later described as the mineral species onoratoite, ideally $Sb_8O_{11}Cl_2$, by Belluomini et al. (1968). This was the first halide found at this locality. According to these authors, the crystallization of quartz was active during the formation of onoratoite, whose temperature of formation should be higher than 60 °C (Belluomini et al., 1968). On the contrary, at ambient temperatures, the crystallization of onoratoite would have been restricted to very specific conditions (Roper et al., 2014). This was a first hint regarding the circulation of late-stage halogen-rich fluids within the Sb ore deposit of the Cetine di Cotorniano.

During the 1980s, the sampling activity of mineral collectors favoured the identification of other halides, represented by fluorides. In addition to fluorite, other species were identified. Among them, the new mineral species rosenbergite, ideally $AlF[F_{0.5}(H_2O)_{0.5}]_4 \cdot H_2O$, was described by Olmi et al. (1993). These fluoride minerals were mainly collected in a small exploitation void known among mineral collectors

as *Stanza Santoni*. There, rare minerals can be found in the cavities of jasperoids (i.e. strongly silicified limestone, black in colour), which are lined by small quartz crystals. In addition to euhedral individuals of some rare species, e.g. elpasolite and hydrokenoralstonite (e.g. Menchetti and Batoni, 2015), rosette-like or (hemi)spherical microcrystalline aggregates can be commonly observed.

An investigation of these aggregates using X-ray powder diffraction techniques identified several mineral species: F-bearing alunite, quartz, and two hitherto unknown species, i.e. nannoniite (IMA 2024-010) and dacostaite (IMA 2024-015). The former is relatively common and was probably misidentified as gibbsite for a long time (Biagioni et al., 2024), whereas dacostaite, described in this paper, is very rare and is currently present in fewer than 10 known specimens. This latter mineral, its name, and its symbol (Dcs) were approved by the Commission on New Minerals, Nomenclature, and Classification of the International Mineralogical Association (CNMNC-IMA). The name honours Angelo Da Costa (1940–2022) for his contributions to the field of mineralogy in Tuscany. Angelo Da Costa was a mineral collector active from the beginning of the 1970s up to his death in 2022. He contributed to the exploration of several mineralogical localities, mainly in northern Tuscany (Apuan Alps, Monte Pisano), where he discovered some new mineral occurrences. He collaborated with the Museo di Storia Naturale of the University of Pisa, providing material for mineralogical studies. The type material for dacostaite is deposited in the collection of the Museo di Storia Naturale, University of Pisa, Via Roma 79, Calci (Pisa), under catalogue number 20073.

This paper describes this new mineral species, discussing its occurrence and crystal chemistry.

2 Occurrence and physical properties

Dacostaite was identified in a specimen collected at the Cetine di Cotorniano Mine (43°13′ N, 11°09′ E), Chiusdino, Siena province, Tuscany, Italy. The Sb ore deposit formerly exploited at this locality is probably related to the circulation of hydrothermal fluids triggered by the geothermal anomaly induced by the Miocene–Quaternary magmatic rocks belonging to the Tuscan magmatic province (e.g. Lattanzi, 1999; Dini, 2003; Sillitoe and Brogi, 2021). Antimony ores, represented almost exclusively by stibnite, are associated with jasperoids and vuggy silica masses replacing host rocks (the *Calcare cavernoso* formation of Upper Triassic age) at the contact with the overlying argillic formations belonging to the Liguride Nappe.

In the type material, dacostaite occurs as aggregates of thin pseudo-hexagonal micaceous, colourless-to-white flakes up to 0.5 mm in size (Fig. 1). The streak is white, and the lustre is silky. Dacostaite is not fluorescent under both short- ($\lambda = 254$ nm) and long-wavelength ($\lambda = 350$ nm) UV radiation. Mohs hardness was not determined owing to the small crystal size; the mineral is probably soft. Dacostaite is brittle, with a perfect {001} cleavage. Crystals are flexible but not elastic. Density was not measured owing to the small amount of available material; the calculated density based on the empirical formula and unit-cell parameters measured through single-crystal X-ray diffraction is 2.162 g cm^{-3}.

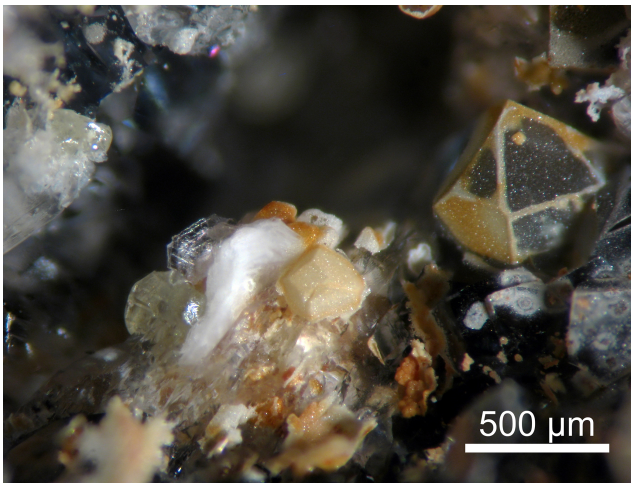

Figure 1. Dacostaite, thin colourless-to-white crystals associated with sulfur, quartz, gypsum, and a pseudomorphosed cube-octahedral crystal of an unknown phase replaced by a microcrystalline pharmacosiderite-like species. Cetine di Cotorniano Mine, Chiusdino, Siena province, Tuscany, Italy. Holotype specimen: Museo di Storia Naturale of the University of Pisa. Catalogue no. 20073. Photo by Cristian Biagioni.

Dacostaite is colourless and non-pleochroic under plane-polarized light. It forms thin laths with a prominent {001} cleavage. Crystals are bent, resulting in undulatory extinction. Extinction is parallel or close to parallel to the cleavage plane. Dacostaite is biaxially negative, with $\alpha = 1.4730(4)$, $\beta = 1.4801(4)$, and $\gamma = 1.4805(4)$, measured using 589 nm light. The angle $2V$ determined from extinction measurements on a spindle stage is 29(2)°, which is in good agreement with the value of 27° calculated by the equation of Wright (1951). Dispersion is weak. The Gladstone–Dale compatibility index (Mandarino, 1979, 1981) is −0.005 (superior).

In the type material, dacostaite is associated with quartz, sulfur, gypsum, and a pharmacosiderite-like mineral in a small cavity of silicified limestone.

3 Experiment

3.1 Raman spectroscopy

Raman spectra of dacostaite were collected in the range of 4000–50 cm^{-1} using a DXR dispersive Raman spectrometer (Thermo Scientific) mounted on a confocal Olympus microscope (Department of Mineralogy and Petrology, National

Museum, Prague, Czech Republic). The Raman signal was excited by an unpolarized red 633 nm He–Ne laser and detected by a charge-coupled device (CCD) detector. The experimental parameters were a 100× objective, a 10 s exposure time, 100 exposures, a 25 µm pinhole spectrograph aperture, and an 8 mW laser power level. The thermal damage of the measured points was excluded by visual inspection of the excited surface after measurement, by observation of possible decay of spectral features at the start of excitation, and by checking for thermal downshift of Raman lines. The instrument was set up with a software-controlled calibration procedure using multiple neon emission lines (wavelength calibration), multiple polystyrene Raman bands (laser frequency calibration), and standardized white-light sources (intensity calibration). Spectral manipulations were performed using the Omnic 9 software (Thermo Scientific).

3.2 Chemical data

Quantitative chemical analyses were carried out using a Cameca SX 100 electron microprobe (wavelength dispersive spectrometer (WDS) mode, 15 kV, 5 nA, 10 µm beam diameter) on carbon-coated, unpolished crystal surfaces at the National Museum in Prague, Czech Republic. Results (average of 10 spot analyses) are given in Table 1. Other elements sought (Si, S, Pb, Cl, Ni, and Co) were below the detection limits. Matrix correction by the PAP algorithm (Pouchou and Pichoir, 1985) was applied to the data.

Raman spectroscopy, as well as structure analysis (see below), indicated the absence of CO_3 groups. Since insufficient pure material is available for a direct determination, the amount of H_2O has been calculated based upon the known stoichiometry from the structure analysis. The wide ranges and high totals of analyses after the addition of calculated H_2O content are caused by the uneven, unpolished sample surface and by the dehydration of the sample under the vacuum of the electron microprobe (loss of six to seven H_2O groups).

3.3 X-ray crystallography

Owing to the small amount of pure material, X-ray powder diffraction data of dacostaite were collected using a Bruker D8 Venture single-crystal diffractometer equipped with a PHOTON III CCD area detector and microfocus Cu$K\alpha$ radiation (Centro per l'Integrazione della Strumentazione scientifica dell'Università di Pisa (CISUP) in Pisa, Italy), simulating Gandolfi-like motion. Observed X-ray diffraction lines are reported in Table 2, along with the calculated pattern based on the structural model discussed below. Unit-cell parameters were refined using the software UnitCell (Holland and Redfern, 1997) and are $a = 12.4760(18)$, $b = 7.1974(11)$, $c = 13.7211(18)$ Å, $\beta = 99.549(12)°$, and $V = 1215.0(2)$ Å^3.

Single-crystal intensity data were collected using a Bruker D8 Venture diffractometer equipped with an air-cooled PHOTON III CCD detector and microfocus Mo$K\alpha$ radiation (CISUP, University of Pisa, Italy). The detector-to-crystal distance was 38 mm. Data were collected using ω and φ scan modes in 0.5° slices, with an exposure time of 30 s per frame. A total of 1024 frames were collected. The frames were integrated with the Bruker SAINT software package using a narrow-frame algorithm. Data were corrected for Lorentz polarization, absorption, and background using the software package Apex4 (Bruker AXS Inc., 2022). Unit-cell parameters were refined on the basis of the XYZ centroid of 952 reflections above $20\sigma(I)$, with $6.558° < 2\theta < 50.98°$. The statistical tests on the distribution of $|E|$ values ($|E^2 - 1| = 0.831$) suggest (but not unequivocally) the occurrence of a centre of symmetry. According to the systematic absences and the uncertainty in the occurrence of a centre of symmetry, the crystal structure of dacostaite was solved in three different space groups using Shelxtl (Sheldrick, 2015a), i.e. $C2/m$, $C2$, and Cm. The main structural features are very similar in these three models. However, the $C2$ and Cm structure models gave racemic twin ratios close to 0.5, suggesting the occurrence of a centre of symmetry. For this reason, the crystal structure of dacostaite was refined using Shelxl-2018 (Sheldrick, 2015b) in the space group $C2/m$. Neutral scattering curves taken from the *International Tables for Crystallography* (Wilson, 1992) were used. A total of 5 independent cation sites (one of them being split) and 10 anion positions (one of them split) were located. Details of the data collection and crystal structure refinement are given in Table 3. Atom coordinates and isotropic or equivalent-isotropic displacement parameters are reported in Table 4, whereas Table 5 gives selected bond distances. Bond-valence calculation, shown in Table 6, was performed using the bond parameters of Brese and O'Keeffe (1991).

4 Results and discussion

4.1 Raman spectrum of dacostaite

The main bands observed in the Raman spectrum of dacostaite in the region between 1000 and 50 cm^{-1} are (in cm^{-1}) 838, 531, 397, 257, 176, and 130 (Fig. 2). The most prominent Raman band at 838 cm^{-1} is attributed to the ν_1 symmetric stretching vibration of AsO_4 groups. The bands at 531 and 397 cm^{-1} may be attributed to the ν_4 and ν_2 bending vibrations of AsO_4 groups, respectively. Finally, bands below 300 cm^{-1} (257, 176, and 130 cm^{-1}) are probably related to (Mg,Al)–φ (φ is OH, F, H_2O) vibrations and lattice modes. The presence of H_2O groups and hydroxyl ions is documented by a broad OH-stretching band running from 3550 to 3100 cm^{-1}, with a maximum at 3278 cm^{-1} (Fig. 2). According to the empirical relation between energy of vibration and the corresponding bond length (Libowitzky, 1999), O–H···O hydrogen bond lengths vary approximately in the

Table 1. Chemical data (in wt %) for dacostaite.

Constituent	Mean	Range ($n = 10$)	Standard deviation (σ)	Normalized	Standard
P_2O_5	0.17	0.02–0.27	0.07	0.14	Fluorapatite
As_2O_5	35.42	34.37–35.98	0.57	28.69	Clinoclase
Al_2O_3	12.23	10.69–13.72	1.01	9.91	Sanidine
MgO	21.13	18.60–24.94	2.13	17.12	Diopside
CaO	0.36	0.27–0.46	0.06	0.29	Fluorapatite
MnO	0.04	0.01–0.08	0.02	0.03	Rhodonite
FeO	0.04	0.00–0.08	0.03	0.03	Hematite
CuO	0.42	0.27 – 0.94	0.19	0.34	Chalcopyrite
ZnO	0.34	0.21–0.47	0.09	0.27	ZnO
Na_2O	0.15	0.05–0.33	0.10	0.12	Albite
K_2O	4.13	2.85–5.43	0.78	3.35	Sanidine
F	13.15	9.13–16.59	2.91	10.65	LiF
Sum	87.58	86.57–88.71	0.78	70.94	
$O = -F$	−5.54			−4.48	
H_2O_{calc}*	41.40			33.54	
Total	123.44			100.00	

Note that n is the number of spot analyses. * Calculated according to stoichiometry.

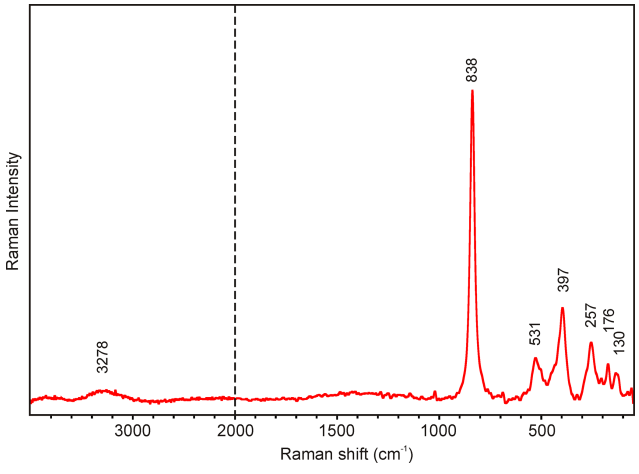

Figure 2. The Raman spectrum of dacostaite in the range in the range of 4000–50 cm^{-1}, split at 2000 cm^{-1}.

range from 2.7 to 2.9 Å (with a maximum of 2.73 Å); these calculated lengths are comparable to the results of the crystal structure study of dacostaite (see below).

4.2 Chemical formula of dacostaite

The empirical formula of dacostaite, which is based on $(As + P) = 2$ atoms per formula unit (apfu), takes into account the results of the crystal structure study (see below), and fixes the (OH)/O ratio in order to achieve the electrostatic balance, is (with rounding errors) $(K_{0.56}Ca_{0.04}Na_{0.03}\square_{0.37})_{\Sigma 1.00}\,(Al_{1.54}Mg_{1.38}Cu_{0.03}Zn_{0.03})_{\Sigma 2.98}\,[Mg(H_2O)_6]_2\,[(As_{0.99}P_{0.01})O_4]_2[F_{4.46}(OH)_{1.46}O_{0.08}]_{\Sigma 6.00} \cdot 2H_2O$.

Following Bosi et al. (2019a, b) and on the basis of this empirical formula, two main possible end-member charge arrangements can be proposed:

i. $R^+(R^{2+}_2R^{3+})[R^{2+}(H_2O)_6]_2[R^{5+}O_4]_2R^-_6 \cdot 2H_2O$ and

ii. $R^0(R^{2+}R^{3+}_2)[R^{2+}(H_2O)_6]_2[R^{5+}O_4]_2R^-_6 \cdot 2H_2O$.

The arrangement $R^+(R^{2+}_2R^{3+})$ would correspond to $(K,Na)_{0.59}(Mg_{1.18}Al_{0.59})$, and it is limited by the $(K + Na)$ content, with $K \gg Na$, whereas the arrangement $R^0(R^{2+}R^{3+}_2)$ would correspond to $\square_{0.37}(Mg_{0.37}Al_{0.74})$, and it is limited by the $\square$ content. Because the first arrangement is more abundant (59 %) than the second, the dominant end-member composition of dacostaite is $K(Mg_2Al)[Mg(H_2O)_6]_2(AsO_4)_2F_6 \cdot 2H_2O$. This corresponds to (in wt %) As_2O_5 28.47, Al_2O_3 6.31, MgO 19.97, K_2O 5.83, F 14.12, H_2O 31.25, $O = -F = -5.95$, sum 100.00.

4.3 Crystal structure of dacostaite

4.3.1 General features

The crystal structure of dacostaite can be described as being formed of heteropolyhedral {001} layers and isolated $Mg(H_2O)_6$ groups connected by H bonds (Fig. 3a, b). The heteropolyhedral layers are composed of octahedrally coordinated atoms hosted at the $M(1)$ and $M(2)$ sites, forming an octahedral layer decorated on both sides by $As(1)O_4$ tetrahedra (Fig. 3c). The octahedral layer can be described as being

Table 2. X-ray powder diffraction data (d in Å) for dacostaite.

I_{obs}	d_{obs}	d_{calc}	I_{calc}	$h\ k\ l$
s	13.7	13.54	100	0 0 1*
w	6.2	6.21	3	1 1 0*
mw	5.98	5.99	8	−2 0 1*
–	–	5.83	2	−1 1 1
m	5.48	5.48	27	1 1 1*
w	4.994	4.980	8	−2 0 2*
w	4.800	4.780	3	−1 1 2*
vw	4.530	4.512	1	0 0 3*
vw	4.216	4.218	1	2 0 2*
vw	3.970	3.964	2	−2 0 3*
vw	3.825	3.805	1	−1 1 3*
		3.599	3	0 2 0
mw	3.581	3.574	3	−3 1 1
		3.563	3	3 1 0
–	–	3.514	6	1 1 3
w	3.339	3.358	2	−3 1 2
		3.330	2	3 1 1
w	3.186	3.196	2	−2 0 4
		3.178	2	0 2 2
vw	3.102	3.106	1	2 2 0*
		2.993	7	−4 0 2
m	2.977	2.974	15	2 2 1*
w	2.911	2.917	2	−2 2 2
		2.873	2	1 1 4
w	2.746	2.763	2	−4 0 3
		2.738	2	2 2 2
w	2.715	2.707	6	0 0 5*
w	2.654	2.665	2	−2 2 3*
vw	2.564	2.561	3	−1 1 5*
vw	2.468	2.464	1	2 2 3*
w	2.385	2.390	3	−2 2 4*
w	2.324	2.328	1	5 1 0*
vw	2.303	2.301	1	−4 2 2*
w	2.244	2.256	1	0 0 6*
w	2.208	2.203	1	1 3 2*
w	2.108	2.103	1	5 1 2*
w	2.070	2.076	1	−5 1 4*
w	2.021	2.022	1	3 3 1*
w	1.973	1.977	1	4 2 3*
w	1.933	1.936	1	3 3 2*
w	1.899	1.898	1	−6 0 4*
mw	1.797	1.800	5	−6 2 1
		1.800	3	0 4 0
w	1.756	1.757	3	2 2 6*

I_{calc} and d_{calc} were obtained using PowderCell 2.4 (Kraus and Nolze, 1996) on the basis of the structural model of dacostaite given in Table 4. Only calculated reflections with $I_{calc} > 1$ (if not observed) are reported. I_{obs} were visually estimated: s is strong, m is medium, mw is medium weak, w is weak, and vw is very weak. The symbol * indicates reflections used for the refinement of unit-cell parameters.

formed of chains of $M(1)$-centred corner-sharing octahedra running along b, connected along a through corner-sharing with $M(2)$-centred octahedra, giving rise to a layer characterized by pseudo-hexagonal and triangular cavities. Potassium atoms are hosted in these pseudo-hexagonal cavities, whereas the O atoms delimiting the triangular cavities are bonded to the tetrahedrally coordinated As^{5+} atoms.

Heteropolyhedral layers and isolated $Mg(H_2O)_6$ groups are connected through H bonds that also involve a free-H_2O group located between {001} layers.

4.3.2 Cation sites

Arsenic and very minor amounts of P are hosted at the As(1) site and show a tetrahedral coordination, with an average ⟨As–O⟩ distance of 1.676 Å, which compares with the value of 1.685 Å given by Majzlan et al. (2014) for the mean As–O distance. The bond-valence sum (BVS) is 5.14 valence units (v.u.), in agreement with the occurrence of As^{5+}.

The $M(1)$- and $M(2)$-centred octahedra have $\langle M–\varphi\rangle$ (φ is F, OH, O) distances of 1.939 and 1.937 Å. Their site occupancies were refined using the scattering curve of Al. However, on the basis of the observed bond distances and electron microprobe data, mixed (Al,Mg) site occupancies can be proposed. Minor amounts of Cu and Zn could be hosted at these positions, but their contents are very low and were not considered in the structural study. Magnesium and Al cannot be definitively distinguished based solely on site scattering due to their similar scattering curves ($Z = 12$ and 13 for Mg and Al, respectively). However, they can be distinguished by examining the observed bond distances. Using the bond-valence parameters of Brese and O'Keeffe (1991), the ideal Al–O, Al–F, Mg–O, and Mg–F bond distances can be calculated (in Å) as 1.907, 1.801, 2.103, and 1.991, respectively. The average distances observed for the $M(1)$- and $M(2)$-centred octahedra support mixed (Al,Mg) occupancies. The $M(1)$ and $M(2)$ sites are coordinated by four F-bearing sites, i.e. F(4) and F(5), and two O-hosting sites, namely O(1) and O(2). While O(1) and O(2) host O^{2-} (see below), the occupancies of F(4) and F(5) are probably represented by mixed (F,OH), in agreement with the electron microprobe analysis showing idealized contents of 4.50 F and 1.50 (OH) groups per formula unit. No indication of preferential partitioning of (OH) groups between F(4) and F(5) was observed (see below), and consequently a disordered distribution of F and (OH) between these two anion positions is assumed. If we assume that the site occupancy at F(4) and F(5) is $[F_{0.75}(OH)_{0.25}]$, then the following site occupancies at $M(1)$ and $M(2)$ can be calculated on the basis of observed bond distances: $M(1) = Al_{0.55}Mg_{0.45}$ and $M(2) = Al_{0.57}Mg_{0.43}$. Considering the site multiplicity, this results in the site population $^{M(1)+M(2)}(Al_{1.67}Mg_{1.33})$, which can be compared to the composition derived from electron microprobe analysis, $^{M(1)+M(2)}(Al_{1.55}Mg_{1.45})$, considering Cu^{2+} and Zn^{2+} as Mg^{2+}. For the calculation of the BVS, the

Table 3. Crystal and experimental data for dacostaite.

Crystal data	
Crystal size (mm)	$0.070 \times 0.040 \times 0.020$
Cell setting, space group	Monoclinic, $C2/m$
a (Å)	12.474(5)
b (Å)	7.198(3)
c (Å)	13.724(6)
β (°)	99.518(13)
V (Å^3)	1215.3(8)
Z	2
Data collection and refinement	
Radiation, wavelength (Å)	Mo$K\alpha$, 0.71073
Temperature (K)	293(2)
$2\theta_{max}$ (°)	52.73
Measured reflections	6874
Unique reflections	1325
Reflections with $F_o > 4\sigma(F_o)$	1022
R_{int}	0.1114
$R\sigma$	0.1007
Range of h, k, l	$-15 \le h15, -8 \le k \le 8, -15 \le l \le 17$
R [$F > 4\sigma(F)$]	0.0927
R (all data)	0.1152
wR (on F^2)	0.2574
GoF	1.055
Number of least-squares parameters	102
Maximum and	2.53 [at 0.79 Å from Ow(3)]
minimum residual peak (e Å^{-3})	−1.32 [at 0.87 Å from As(1)]

Table 4. Sites, Wyckoff positions, site occupancy (s.o.), fractional atom coordinates, and equivalent-isotropic or isotropic (*) displacement parameters (in Å^2) for dacostaite.

Site	Wyckoff position	s.o.	x/a	y/b	z/c	$U_{eq/iso*}$
K(1)	2a	$K_{0.43(2)}$	0	0	0	0.011(2)*
K(2)	4i	$K_{0.209(9)}$	0.0065(9)	0	0.0398(14)	0.011(2)*
As(1)	4i	$As_{1.00}$	0.63298(10)	0	0.81461(11)	0.0204(5)
M(1)	4e	$Al_{1.00}$	1/4	3/4	0	0.0195(9)
M(2)	2b	$Al_{1.00}$	1/2	0	0	0.0172(11)
Mg(3)	4i	$Mg_{1.00}$	0.4427(4)	1/2	0.6872(4)	0.0339(13)
Ow(1)	4i	$O_{1.00}$	0.2890(10)	1/2	0.5982(10)	0.057(4)
Ow(2)	4i	$O_{1.00}$	0.5963(11)	1/2	0.7713(12)	0.064(4)
Ow(3)	8j	$O_{1.00}$	0.3894(7)	0.7167(15)	0.7761(10)	0.066(3)
Ow(4)	8j	$O_{1.00}$	0.4941(10)	0.2869(15)	0.6017(8)	0.064(3)
Ow(5a)	4i	$O_{0.333}$	0.194(3)	1/2	0.407(3)	0.041(6)*
Ow(5b)	4i	$O_{0.333}$	0.242(4)	1/2	0.391(3)	0.041(6)*
Ow(5c)	8j	$O_{0.167}$	0.254(4)	0.582(8)	0.404(4)	0.041(6)*
O(1)	8j	$O_{1.00}$	0.7050(5)	0.1903(9)	0.8558(5)	0.0239(15)
O(2)	4i	$O_{1.00}$	0.5120(7)	0	0.8553(8)	0.023(2)
O(3)	4i	$O_{1.00}$	0.6108(8)	0	0.6932(9)	0.035(3)
F(4)	8j	$F_{1.00}$	0.3916(4)	0.8130(8)	0.9759(4)	0.0255(12)
F(5)	4i	$F_{1.00}$	0.2042(6)	0	0.9761(6)	0.0263(18)

Table 5. Selected bond distances (in Å) in dacostaite.

K(1)	–F(4) × 4	2.620(5)	K(2)	–F(5)	2.602(13)	As(1)	–O(3)	1.644(13)
	–F(5) × 2	2.622(8)		–F(4) × 2	2.613(8)		–O(1) × 2	1.684(6)
	Average	2.621		–F(4) × 2	2.735(10)		–O(2)	1.693(9)
				–F(5)	2.750(14)		Average	1.676
				–Ow(3) × 2	3.068(19)			
				–Ow(2)	3.08(2)			
				Average	2.807			
M(1)	–F(5) × 2	1.900(3)	*M*(2)	–F(4) × 4	1.898(5)	Mg(3)	–Ow(2)	2.066(14)
	–F(4) × 2	1.905(5)		–O(2) × 2	2.016(10)		–Ow(4) × 2	2.095(10)
	–O(1) × 2	2.013(7)		Average	1.937		–Ow(1)	2.096(13)
	Average	1.939					–Ow(3) × 2	2.152(13)
							Average	2.109

Table 6. Weighted bond valences (in v.u.) for dacostaite.

Site	K(1)	K(2)	As(1)	*M*(1)	*M*(2)	Mg(3)	Σ_{anions}	Hydrogen bonds	Σ_{anions}*
Ow(1)						0.34	0.34	−0.20, −0.23[a]	−0.09
								−0.20, −0.18[b]	−0.04
								−0.20, −0.23[c]	−0.09
Ow(2)		0.02				0.36	0.38	−0.20, −0.20	−0.02
Ow(3)		$0.02^{\downarrow\times2}$				$0.29^{\downarrow\times2}$	0.31	−0.22, −0.24, +0.09[d]	−0.06
								−0.22, −0.24, +0.10[e]	−0.05
								−0.22, −0.24, +0.11[f]	−0.04
Ow(4)						$0.34^{\downarrow\times2}$	0.34	−0.22, −0.18, +0.11[g]	0.05
								−0.22, −0.18, +0.09[h]	0.03
								+0.18, −0.22, −0.11[i]	0.19
								+0.18, −0.22, −0.09[j]	0.21
Ow(5a)						–	–	+0.23, +0.11, −0.11, −0.09	0.14
Ow(5b)						–	–	+0.18, −0.10, −0.09	−0.01
Ow(5c)						–	–	+0.23, +0.11, −0.09, −0.12[k]	0.13
								+0.23, +0.11, −0.11, −0.12[l]	0.11
								+0.23, −0.11, −0.11[m]	0.01
								+0.23, −0.11, −0.12[n]	0.00
O(1)			$1.25^{\downarrow\times2}$	$0.40^{\downarrow\times2}$			1.66	+0.20, +0.22	2.02
O(2)			1.22		$0.39^{\downarrow\times2}$		1.62	+0.24, +0.24	2.10
O(3)			1.39				1.40	+0.20, +0.22, +0.22	2.04
F(4)	$0.09^{\downarrow\times2}$	$0.04^{\downarrow\times2}$		$0.43^{\downarrow\times2}$	$0.44^{\downarrow\times4}$		1.03		
		$0.03^{\downarrow\times2}$							
F(5)	$0.09^{\downarrow\times4}$	0.04		$2\times\rightarrow0.44^{\downarrow\times2}$			1.04		
		0.03							
$\Sigma_{cations}$	0.54	0.27	5.11	2.54	2.54	1.94			
Theor.	0.43	0.21	5.00	2.55	2.57	2.00			

Note that the * indicates a correction for H bonds (see Table 7). [a] Ow(1) is a donor to Ow(5a). [b] Ow(1) is a donor to Ow(5b). [c] Ow(1) is a donor to Ow(5c). [d,e,f] Ow(3) is a donor to O(1) and O(2) and an acceptor from Ow(5a), Ow(5b), and Ow(5c). [g] Ow(4) is a donor to O(3) and Ow(4) and an acceptor from Ow(5a). [h] Ow(4) is a donor to O(3) and Ow(4) and an acceptor from Ow(5c). [i] Ow(4) is an acceptor from Ow(4) and a donor to O(3) and Ow(5a). [j] Ow(4) is an acceptor from Ow(4) and a donor to O(3) and Ow(5c). [k] Ow(5c) is an acceptor from Ow(1) and Ow(4) and a donor to Ow(2) and Ow(3). [l] Ow(5c) is an acceptor from Ow(1) and Ow(4) and a donor to Ow(1) and Ow(3). [m] Ow(5c) is an acceptor from Ow(1) and a donor to Ow(4) and Ow(3). [n] Ow(5c) is an acceptor from Ow(1) and a donor to Ow(4) and Ow(1). Left and right superscripts indicate the number of bonds involving anions and cations, respectively.

composition based on bond distances was used. The BVSs at *M*(1) and *M*(2) are 2.52 and 2.53 v.u., respectively, in agreement with the mixed (Al,Mg) site occupancies.

The Mg(3) site is occupied by Mg^{2+}, coordinated by six H_2O groups. It has an average ⟨*M*–O⟩ distance of 2.109 Å, in agreement with the occupancy of this position by Mg, as also supported by the BVS value (1.94 v.u.).

Potassium atoms, as well as minor amounts of Ca and Na, are hosted at the split positions K(1) and K(2). The former shows a 6-fold coordination, whereas atoms at K(2) have six short distances (shorter than 2.8 Å) and three longer

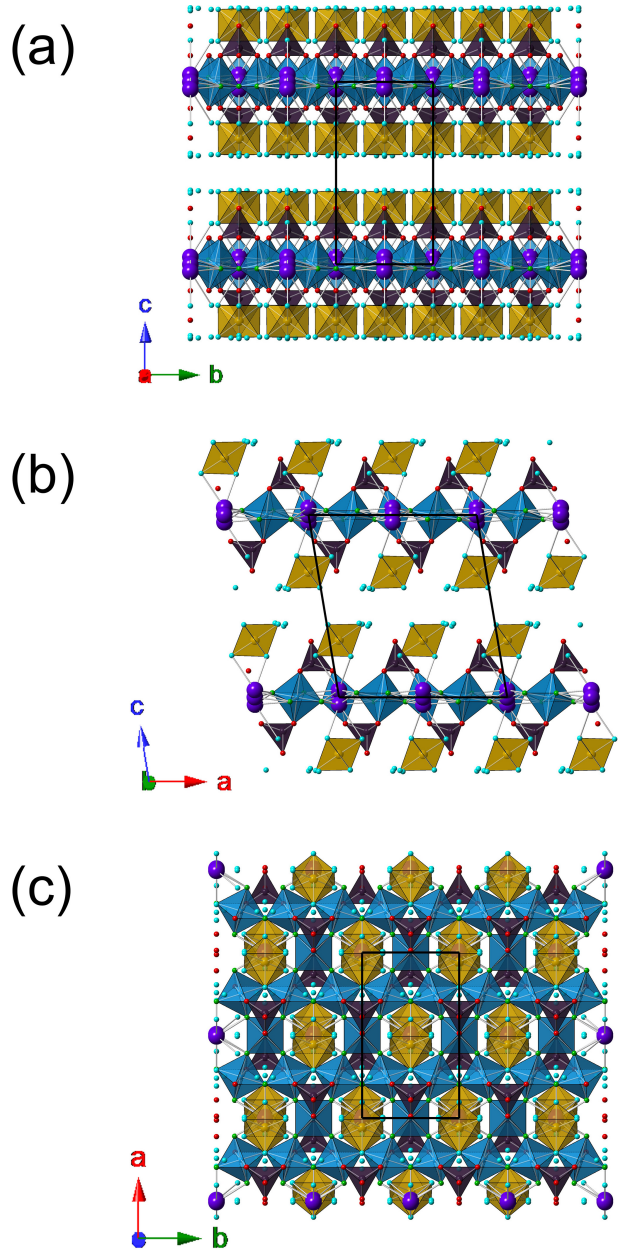

Figure 3. Crystal structure of dacostaite as seen from *a* **(a)**, *b* **(b)** and *c* **(c)**. The symbols are as follows: blue polyhedra are *M*(1)- and *M*(2)-centred octahedra, brown indicates Mg(3)-centred polyhedra, and violet indicates As(1)-centred tetrahedra. The circles are as follows: red indicates O sites, light blue indicates H_2O groups, green indicates F sites, and violet indicates K sites. The unit cell is shown as solid black lines.

ones to H_2O groups of the $Mg(H_2O)_6$-isolated octahedra. The K(1) and K(2) positions cannot be simultaneously occupied, as the K(1)–K(2) distance is 0.539(19) Å, and the K(2)–K(2) distance is 1.08(4) Å. The refined mean atomic number at K(1) + 2K(2) is ∼ 16 electrons, compared to the mean atomic number calculated on the basis of electron microprobe analysis, i.e. ∼ 12 electrons. This discrepancy will be discussed below.

4.3.3 Anion sites and possible H bonds

Ten anion sites have been located in the crystal structure of dacostaite. Bond-valence sums (Table 6) identify three different groups of anions: (i) O(1), O(2), and O(3) have BVSs in the range of 1.40–1.66 v.u.; (ii) F(4) and F(5) have BVSs of ca. 1 v.u.; and (iii) Ow(1) to Ow(5) show BVSs in the range of 0–0.38 v.u. The examination of the O···O distances and O···O···O angles (Table 7) allows us to infer the H-bond network in dacostaite.

The atoms hosted at the O(1), O(2), and O(3) sites belong to the (AsO_4) groups. They are at H-bond distances from the H_2O groups belonging to the $Mg(H_2O)_6$-isolated octahedra. The atom at O(1) is an acceptor of H bonds from Ow(2) and Ow(3); O(2) accepts H bonds from two Ow(2) groups; and O(3) is involved in three H bonds, accepting bonds from Ow(1) and two Ow(4) groups. The bond strengths of these bonds, calculated in agreement with Ferraris and Ivaldi (1988), increase the BVSs at these three positions to values ranging between 2.02 and 2.10 v.u., thus confirming the occurrence of O^{2-} at O(1), O(2), and O(3).

The anions at the Ow(1), Ow(2), Ow(3), and Ow(4) sites are bonded to Mg^{2+}, whereas the split Ow(5) site (actually represented by three sub-positions with fixed site occupancy) is an H_2O group not bonded to any cation. While the H bonds between H_2O groups and O^{2-} atoms belonging to the (AsO_4) groups are well-resolved, the bonds involving H_2O groups only (and in particular the split Ow(5) site) are less constrained, and some uncertainties still remain. According to Ferraris and Franchini-Angela (1972), the O···O distances should be in the range of 2.60–3.20 Å, and the O···O···O angles should be close to 108°, varying between ∼ 80 and ∼ 140°; Table 7 shows that some O···O distances involving the split Ow(5) site are longer than 3.20 Å. Moreover, the bond angles involving this latter split position may be, in some configurations, close to ∼ 80°. Smaller angles have not been considered possible H bonds. Table 6 considers some possible H bonds, giving the corrected sum of bond valences at anions sites and calculating the bond strengths according to Ferraris and Ivaldi (1988).

F(4) and F(5) were refined as pure F sites. During the calculation of BVSs, they were considered mixed (F,OH) sites, in accordance with electron microprobe analysis, which assumed a statistical occupancy [$F_{0.75}(OH)_{0.25}$] at both positions, as no indication of a preferential partitioning of (OH)

Table 7. Hydrogen bonds in dacostaite.

Donor···acceptor	d (Å)	Bond strength (v.u.)
Ow(1)···O(3)	2.756(18)	0.20
Ow(1)···Ow(5a)	2.70(4)	0.23
Ow(1)···Ow(5b)	2.81(5)	0.18
Ow(1)···Ow(5c)	2.69(4)	0.23
Ow(2)···O(1)	2.763(10)	0.20
Ow(3)···O(1)	2.711(11)	0.22
Ow(3)···O(2)	2.670(13)	0.24
Ow(4)···O(3)	2.712(13)	0.22
Ow(4)···Ow(4)	2.82(2)	0.18
Ow(4)···Ow(5a)	3.11(3)	0.11
Ow(4)···Ow(5c)	3.30(6)	0.09
Ow(5a)···Ow(3)	3.27(3)	0.09
Ow(5a)···Ow(4)	3.11(3)	0.11
Ow(5b)···Ow(2)	3.24(5)	0.10
Ow(5b)···Ow(3)	3.29(4)	0.09
Ow(5c)···Ow(1)	3.06(6)	0.12
Ow(5c)···Ow(3)	3.15(6)	0.11
Ow(5c)···Ow(2)	3.33(6)	0.09
Acceptor···donor···acceptor		**Bond angle (°)**
O(3)···Ow(1)···Ow(5a)		101.7(10)
O(3)···Ow(1)···Ow(5b)		115.5(11)
O(3)···Ow(1)···Ow(5c)		117.1(13)
O(1)···Ow(2)···O(1)		107.6(5)
O(2)···Ow(3)···O(1)		110.9(5)
O(3)···Ow(4)···Ow(4)		110.3(5)
O(3)···Ow(4)···Ow(5a)		81.7(6)
O(3)···Ow(4)···Ow(5c)		77.8(11)
Ow(3)···Ow(5a)···Ow(4)		104.1(11)
Ow(2)···Ow(5b)···Ow(3)		79.6(9)
Ow(1)···Ow(5c)···Ow(2)		106.6(10)
Ow(3)···Ow(5c)···Ow(4)		105.6(16)
Ow(4)···Ow(5c)···Ow(1)		83.3(14)
Ow(2)···Ow(5c)···Ow(3)		80.1(14)

at one of these sites was observed (e.g. the U_{eq} values are similar for both sites).

In conclusion, notwithstanding some uncertainties in the actual H-bond system, it is possible to identify O^{2-}-, (H_2O)-, and $(F,OH)^{-}$-bearing sites in the crystal structure of dacostaite.

4.3.4 Crystal chemistry of dacostaite

The formula from the structural refinement of dacostaite can be written as $^{K(1)+K(2)}(K_{0.85}\square_{0.15})^{M(1)+M(2)}_{\Sigma 1.00}(Al_{1.67}Mg_{1.33})_{\Sigma 3.00}$ $[^{Mg(3)}Mg(H_2O)_6]_2(AsO_4)_2F_6 \cdot 2H_2O$ ($Z = 2$). This formula is not charge balanced and has an excess of 0.51 positive charges due to higher amounts of both refined K content and calculated Al content. Indeed, on the basis of the refined K content, the Al content should be lower, i.e. $(Al_{1.15}Mg_{1.85})$, in agreement with the substitution mechanism $K^+ + Mg^{2+} = \square + Al^{3+}$.

Electron microprobe analysis gave the empirical formula $(K_{0.56}Ca_{0.04}Na_{0.03}\square_{0.37})_{\Sigma 1.00}$ $(Al_{1.54}Mg_{1.38}Cu_{0.03}$ $Zn_{0.03})_{\Sigma 2.98}$ $[Mg(H_2O)_6]_{2.00}$ $[(As_{0.99}P_{0.01})O_4]_2$ $[F_{4.46}(OH)_{1.46}O_{0.08}]_{\Sigma 6.00} \cdot 2H_2O$. In this formula, 0.08 O apfu is calculated in order to achieve electrostatic balance. The Al/(Mg + Al) atomic ratio derived from chemical data is 0.313, compared to the value calculated from structure analysis, i.e. 0.334. These values are quite similar, and consequently, the main problem seems to be related to the high refined K content. It is worth noting that if vacancies are replaced by H_2O groups, a total of 14.73 electrons can be calculated for the K(1) + K(2) sites, compared to the 16.15 electrons per formula unit based on structure refinement. Considering the observed bond distances, the occurrence of H_2O groups at K(1) and K(2) is physically reasonable. Therefore, it is reasonable to give the general formula of dacostaite as $[K_{1-x}(H_2O)_x](Mg_{2-x}Al_{1+x})[Mg(H_2O)_6]_2(AsO_4)_2$ $F_{6-y}(OH)_y \cdot 2H_2O$. For the material studied, $x \approx 0.5$ and $y \approx 1.5$.

4.4 Relationships with other species

4.4.1 Structurally related minerals

The octahedral {001} layer of dacostaite can be compared to those occurring in alunite-supergroup minerals, e.g. in crandallite (Blount, 1974) (Fig. 4). Similarity is also seen in the linkage between (TO_4) tetrahedra and the octahedral layers, with each TO_4 tetrahedron sharing three corners with three M-centred octahedra common to a triangular ring. The same kind of heteropolyhedral module was observed in elliottite, ideally $NaAl_3[Mg(H_2O)_6](PO_4)_2F_6 \cdot 3H_2O$ (Grey et al., 2022), where the octahedral sites host Al with minor substitutions of Mg. Moreover, elliottite shares the same pseudo-hexagonal morphology with dacostaite, as a macroscopic expression of the similar C-centred orthohexagonal translations of ca. $7.0\sqrt{3} \times 7.0$ Å. The crandallite-like $[Al_3(PO_4)_2(F,OH)_6]^{3-}$ layer is decorated with (PO_4) groups. Also similar is the coordination of the alkali cation: Na^+ in elliottite and K^+ in dacostaite. Differences can be found in the interlayer, where single-$Mg(H_2O)_6$ octahedra occur in dacostaite, whereas elliottite has dimers of half-occupied $Mg(H_2O)_6$ octahedra, with a basal spacing of ca. 11.1 Å, which is shorter than that in dacostaite, ca. 13.5 Å. Other related phases are penriceite, $[Mg(H_2O)_6][Na(H_2O)_2Al_3(PO_4)_2F_6] \cdot H_2O$, and its (OH)-analogue aldermanite (Elliott et al., 2021, 2022), whose heteropolyhedral layer is different. There is also a chemical similarity to the recently described new mineral chinnerite, $[Mg(H_2O)_6][Na(H_2O)_2Al_3(PO_4)_2F_6]$ (Elliott et al., 2024).

The octahedral layer of dacostaite is also topologically similar to the distorted-hexagonal tungsten bronze sheets oc-

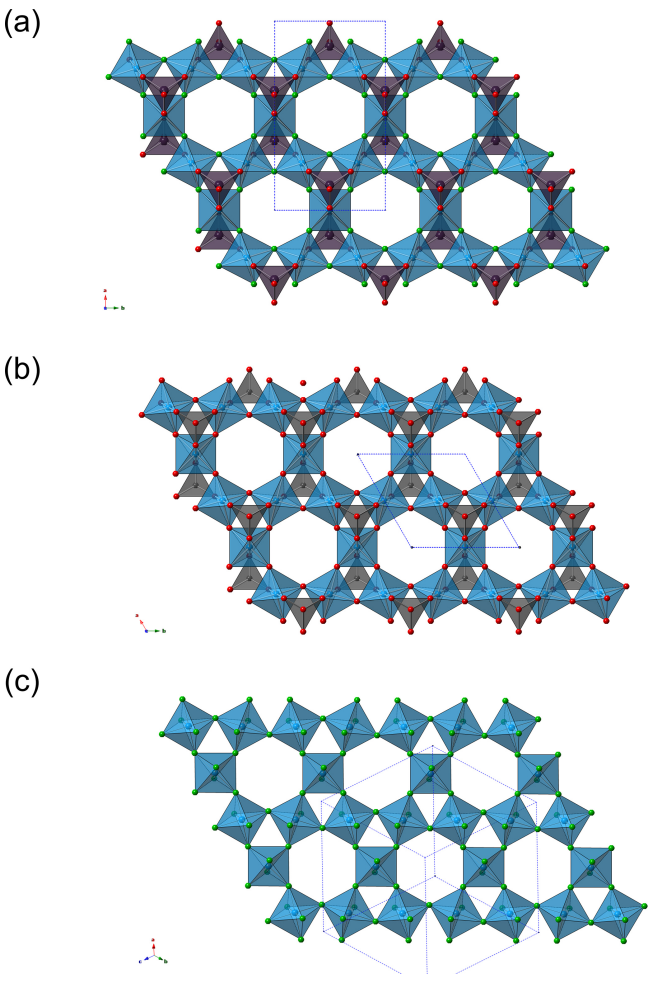

Figure 4. Comparison between the {001} heteropolyhedral layer in dacostaite **(a)**, the octahedral–tetrahedral layer of crandallite (alunite-supergroup minerals) **(b)**, and the tungsten bronze sheet in hydrokenoralstonite (pyrochlore-supergroup minerals) **(c)**. The symbols are the same as in Fig. 3. The unit cells are shown as dotted blue lines.

curring in pyrochlore-supergroup minerals (Fig. 4), in accordance with previous works (e.g. Goreaud and Raveau, 1980). It is noteworthy that the pyrochlore-supergroup mineral hydrokenoralstonite is also reported to occur at the Cetine di Cotorniano Mine (Menchetti and Batoni, 2015).

4.4.2 Natural fluoride arsenates: a short review

Dacostaite is the first mineral species belonging to the K_2O–MgO–Al_2O_3–As_2O_5–H_2O–F system. Arsenic has an average upper-crustal content of ca. 2 µg g^{-1} (Wedepohl, 1995), but it is characterized by geochemical behaviour favouring its occurrence as an essential chemical constituent in more than 600 mineral species (e.g. Majzlan et al., 2014). Indeed, it is one of the elements with the highest diversity index, as defined by Christy (2015). However, only a few arsenates are also characterized by the presence of F as an essential chemical constituent (Table 8). Among the 15 known species, 8 have been described after the year 2000.

These recent findings were related to the discovery of the exceptional fumarolic–arsenate assemblages at the Arsenatnaya fumarole at the second scoria cone of the northern breakthrough of the Great Tolbachik Fissure Eruption, Tolbachik volcano, Kamchatka, Russia (Pekov et al., 2018a). There, five fluoride–arsenate minerals have been identified: arsenowagnerite (Pekov et al., 2018b), axelite (Pekov et al., 2023), evseevite (Pekov et al., 2020a), lehmannite (Pekov et al., 2020b), and polyarsite (Pekov et al., 2020c). All these species are still endemic to the Arsenatnaya fumarole, whereas three other fluoride–arsenates have been reported elsewhere, i.e. durangite, svabite, and tilasite (Pekov et al., 2018a). Svabite and tilasite were both first described from the calc–silicate rocks of the Långban mining district, Sweden, at the end of the 19th century (Sjögren, 1891, 1892, 1895); later discoveries of these minerals from hydrothermal settings associated with Mn ores are known (e.g. Majzlan et al., 2014, and references therein). Durangite is isotypic with tilasite and was first reported from a tin placer in Durango, Mexico (Brush, 1869); according to Foord et al. (1985) and Wilson (1986), this mineral is associated with rhyolites and "tin granites", and its crystallization could be related to paleo-fumarolic activity. The Fe^{3+} analogue of durangite, maxwellite, occurs in the same geological environment (Foord et al., 1991), as well as esperanzaite, which was found in a tin-bearing rhyolite exploited by La Esperanza Mine, Durango, Mexico (Foord et al., 1999).

Fluorine and arsenate groups are also chemical constituents of the borosilicate minerals belonging to the vicanite group. Vicanite–(Ce) was found only in thermometamorphic volcanic ejecta from Latium (Italy) (e.g. Maras et al., 1995), whereas arrheniusite–(Ce) is a recently described mineral from the Östanmossa Mine, one of the Bastnäs-type deposits in the Bergslagen ore region, Sweden, where it occurs in metasomatic F-rich skarn (Holtstam et al., 2021).

Two uranyl arsenates, arsenuranospathite and chistyakovaite, also contain F. The former was originally described by Walenta (1978) as an F-free mineral; only later did studies indicate the presence of F (e.g. Chukanov et al., 2009). Chemically related to arsenuranospathite is chistyakovaite (Chukanov et al., 2006). Both minerals have been described from the oxidation zone of a few U ore deposits.

Finally, dacostaite is the last addition to the short list of fluoride–arsenate minerals.

4.5 Genesis of dacostaite

Dacostaite was found in small cavities of the silicified limestone associated with the Sb ore deposit at the Cetine di Cotorniano Mine. Its genesis may be related to the circulation of

Table 8. Arsenate minerals with F as an essential chemical constituent.

Mineral	Chemical formula	a (Å)	b (Å)	c (Å)	α (°)	β (°)	γ (°)	s.g.	IMA number	Ref.
Arrheniusite–(Ce)	$CaMg[(Ce_7Y_3)Ca_5](SiO_4)_3(Si_3B_3O_{18})(AsO_4)(BO_3)F_{11}$	10.81	10.81	27.52	90	90	120	$R3m$	2019-086	[1]
Arsenowagnerite	$Mg_2(AsO_4)F$	9.86	12.98	12.33	90	109.3	90	$P2_1/c$	2014-100	[2]
Arsenuranospathite	$Al(UO_2)_2(AsO_4)_2F \cdot 20H_2O$	29.93	7.13	7.19	90	90	90	$Pmn2$	1982 s.p. ?	[3]
Axelite	$Na_{14}Cu_7(AsO_4)_8F_2Cl_2$	14.60	14.60	8.34	90	90	90	$P4bm$	2017-015a	[4]
Chistyakovaite	$Al(UO_2)_2(AsO_4)_2F \cdot 6.5H_2O$	19.99	9.79	19.62	90	110.7	90	$P2/m$, $P2$, or Pm	2005-003	[5]
Dacostaite	$K(Mg_2Al)[Mg(H_2O)_6]_2(AsO_4)_2F_6 \cdot 2H_2O$	12.47	7.20	13.72	90	99.5	90	$C2/m$	2024-015	[6]
Durangite	$NaAl(AsO_4)F$	6.58	8.51	7.02	90	115.4	90	$C2/c$	G	[7]
Esperanzaite	$NaCa_2Al_2(AsO_4)_2F_4(OH) \cdot 2H_2O$	9.69	10.74	5.55	90	105.3	90	$P2_1/m$	1998-025	[8]
Evseevite	$Na_2Mg(AsO_4)F$	5.32	14.12	12.00	90	90	90	$Pbcn$	2019-064	[9]
Lehmannite	$Na_{18}Cu_{12}TiO_8(AsO_4)_8FCl_5$	10.82	21.11	11.86	90	117.1	90	$C2/m$	2017-057a	[10]
Maxwellite	$NaFe^{3+}(AsO_4)F$	6.67	8.78	7.13	90	114.5	90	$C2/c$	1987-044	[11]
Polyarsite	$Na_7CaMgCu_2(AsO_4)_4F_2Cl$	8.43	10.10	10.71	90	90.8	90	$I2/m$	2019-058	[12]
Svabite	$Ca_5(AsO_4)_3F$	9.73	9.73	6.98	90	90	120	$P6_3/m$	G	[13]
Tilasite	$CaMg(AsO_4)F$	6.68	8.95	7.57	90	121.1	90	$C2/c$	G	[14]
Vicanite–(Ce)	$(Ca,Ce,La,Th)_{15}As^{5+}(As^{3+},Na)_{0.5}Fe^{3+}_{0.7}Si_6B_4(O,F)_{47}$	10.81	10.81	27.33	90	90	120	$R3m$	1991-050	[15]

[1] Holtstam et al. (2021); [2] Pekov et al. (2018b); [3] Dal Bo et al. (2015); [4] Pekov et al. (2023); [5] Chukanov et al. (2006); [6] this work; [7] Downs et al. (2012); [8] Foord et al. (1999); [9] Pekov et al. (2020a); [10] Pekov et al. (2020b); [11] Cooper and Hawthorne (1995); [12] Pekov et al. (2020c); [13] Biagioni et al. (2016); [14] Bermanec (1994); and [15] Ballirano et al. (2002). s.g. stands for space group. G stands for grandfathered. s.p. stands for special procedure.

late-stage, probably oxidized (Al,F)-rich fluids, as indicated by the occurrence of As^{5+} in dacostaite.

It is worth noting that in the same occurrence, other fluoride minerals have been found, i.e. elpasolite, fluorite, gearksutite, hydrokenoralstonite, nannoniite, and rosenbergite, and the F-enrichment of alunite was observed (Biagioni et al., 2024). Considering the crystal chemistry of these phases, it is probable that these (Al,F)-bearing fluids were also enriched in Na, K, Mg, and Ca. We hypothesize that late-stage, low-T hydrothermal fluids leached F as well as alkali- and alkaline-earth metals from the phyllitic basement underlying the silicified limestones; another potential source (in particular of alkalis) could be the evaporitic rocks occurring in this deposit, in accordance with previous observations in some active geothermal fields in Tuscany (e.g. Morteani et al., 2017). To the best of our knowledge, no geochemical data are available for the F content in the host rocks of the Cetine di Cotorniano Mine; nevertheless, the crystallization of F-bearing sulfates on phyllites in the lower mining levels, i.e. rostite and uklonskovite (Sabelli, 1984, 1985), suggests the availability of F in phyllitic rocks.

Dacostaite is more complex than the other fluorides previously found at the Cetine di Cotorniano Mine because it also contains As^{5+}. Arsenate minerals are relatively rare at this locality, and only pharmacosiderite and scorodite are currently known (Menchetti and Batoni, 2015, and references therein). As outlined by Menchetti and Batoni (2015), no arsenopyrite or other primary As-bearing minerals whose alteration could give rise to these phases are known in association with these arsenate minerals. However, although geochemical data are still limited, pyrite from the Hg–Sb ores from southern Tuscany seems to be As enriched (e.g. D'Orazio et al., 2017) and could be a possible source of As. Sillitoe and Brogi (2021) stressed that As values up to 2000 $\mu g\,g^{-1}$ have been found in Sb ores without visible arsenopyrite or As sulfides, thus suggesting the possible As-rich nature of Fe sulfides. Finally, dacostaite shows very minor amounts of Cu and Zn, which suggests that hydrothermal fluids interacted with the ores.

5 Conclusion

The Cetine di Cotorniano Mine is one of the most important geosites in Tuscany, owing to the occurrence of a series of interesting mineral species. Since the first description of onoratoite (Belluomini et al., 1968), mineral collectors have explored and sampled this site, leading to the discovery of several other new mineral species, from both metallurgical slag (cetineite and brizziite – Sabelli and Vezzalini, 1987; Olmi and Sabelli, 1994) and the cavities of jasperoids (rosenbergite – Olmi et al., 1993). The advancements in mineralogical crystallography driven by technological progress in laboratory instruments allowed the recent description of batoniite

(Mauro et al., 2023), nannoniite (Biagioni et al., 2024), and dacostaite.

The discovery of these new phases improves our knowledge of mineral systematics and crystal chemistry and provides the description of new crystal structure arrangements. This is the case with dacostaite, which is the first potassium–aluminium–magnesium–fluoride–arsenate mineral and has a new structure type. It is interesting to note that some modules of its layered structure are known in other phases (alunite-supergroup minerals, pyrochlore-supergroup minerals), confirming the words of Galileo Galilei (1564–1642) reported by Ferraris et al. (2008) in the introduction of their book on modular crystallography: "Nature does not act by means of many things when it can do so by means of few". Moreover, dacostaite opens new questions about the nature of the late-stage fluids circulating within the Cetine di Cotorniano Sb-ore deposit, suggesting the necessity of further studies to understand the details of the ore genesis of Sb(Au) deposits from Tuscany.

Data availability. The crystallographic information file for dacostaite is available in the Supplement.

Supplement. The supplement related to this article is available online at: https://doi.org/10.5194/ejm-37-39-2025-supplement.

Author contributions. CB, DM, and AD collected the preliminary data. CB carried out single-crystal X-ray diffraction. JS collected micro-Raman data. JS and ZD performed the electron microprobe analysis. RS collected optical data. CB wrote the paper, with inputs from the other authors.

Competing interests. At least one of the (co-)authors is a member of the editorial board of *European Journal of Mineralogy*. The peer-review process was guided by an independent editor, and the authors also have no other competing interests to declare.

Disclaimer. Publisher's note: Copernicus Publications remains neutral with regard to jurisdictional claims made in the text, published maps, institutional affiliations, or any other geographical representation in this paper. While Copernicus Publications makes every effort to include appropriate place names, the final responsibility lies with the authors.

Special issue statement. This article is part of the special issue "New minerals: EJM support". It is not associated with a conference.

Acknowledgements. Massimo Batoni is acknowledged for providing us with the specimen of dacostaite used for this mineralogical investigation. The comments of Anthony R. Kampf and an anonymous reviewer helped us in improving the original paper.

Financial support. This research has been supported by the Ministry of Culture of the Czech Republic with a grant to Jiří Sejkora and Zdeněk Dolníček (long-term project DKRVO 2024-2028/1.II.b; National Museum, 00023272).

Review statement. This paper was edited by Sergey Krivovichev and reviewed by Anthony Kampf and one anonymous referee.

References

Ballirano, P., Callegari, A., Caucia, F., Maras, A., Mazzi, F., and Ungaretti, L.: The crystal structure of vicanite-(Ce), a borosilicate showing an unusual $(Si_3B_3O_{18})^{15-}$ polyanion, Am. Mineral., 87, 1139–1143, 2002.

Belluomini, G., Fornaseri, M., and Nicoletti, M.: Onoratoite, a new antimony oxychloride from Cetine di Cotorniano, Rosia (Siena, Italy), Mineral. Mag., 36, 1037–1044, 1968.

Bermanec, V.: Centro-symmetric tilasite from Nežilovo, Macedonia: A crystal structure refinement, Neues Jb. Miner. Monat., 1994, 289–294, 1994.

Biagioni, C., Bosi, F., Hålenius, U., and Pasero, M.: The crystal structure of svabite, $Ca_5(AsO_4)_3F$, an arsenate member of the apatite supergroup, Am. Mineral., 101, 1750–1755, 2016.

Biagioni, C., Mugnaioli, E., Lorenzon, S., Mauro, D., Musetti, S., Sejkora, J., Belmonte, D., Demitri, N., and Dolníček, Z.: Nannoniite, $Al_2(OH)_5F$, a new mineral from the Cetine di Cotorniano mine (Tuscany, Italy), Eur. J. Mineral., 36, 1011–1022, https://doi.org/10.5194/ejm-36-1011-2024, 2024.

Blount, A. M.: The crystal structure of crandallite, Am. Mineral., 59, 41–47, 1974.

Bosi, F., Biagioni, C., and Oberti, R.: On the chemical identification and classification of minerals, Minerals, 9, 591, https://doi.org/10.3390/min9100591, 2019a.

Bosi, F., Hatert, F., Hålenius, U., Pasero, M., Miyawaki, R., and Mills, S. J.: On the application of the IMA-CNMNC dominant-valency rule to complex mineral compositions, Mineral. Mag., 83, 627–632, 2019b.

Brese, N. E. and O'Keeffe, M.: Bond-valence parameters for solids, Acta Crystallogr. B, 47, 192–197, 1991.

Bruker AXS Inc.: APEX4, Bruker Advanced X-ray Solutions, Madison, Wisconsin, USA, 2022.

Brush, G. J.: On durangite, a fluo-arsenate from Durango in Mexico, Am. J. Sci. Arts, 98, 179–182, 1869.

Christy, A. G.: Causes of anomalous mineralogical diversity in the Periodic Table, Mineral. Mag., 79, 33–49, 2015.

Chukanov, N. V., Sidorenko, G. A., Naumova, I. S., Zadov, A. E., and Kuz'min, V. I.: Chistyakovaite, a new mineral $Al(UO_2)_2(AsO_4)_2(F,OH)\cdot 6.5H_2O$, Dokl. Earth Sci., 407, 290–293, 2006.

Chukanov, N. V., Möckel, S., Sidorenko, G. A., and Zaitsev, V. A.: Arsenuranospathite, $Al(UO_2)_2(AsO_4)_2F\cdot 20H_2O$: Formula revision and relationships with allied uranyl arsenates and phosphates, Neues Jb. Miner. Abh., 185, 305–312, 2009.

Cooper, M. A. and Hawthorne, F. C.: The crystal structure of maxwellite, Neues Jb. Miner. Monat., 1995, 97–104, 1995.

Dal Bo, F., Hatert, F., Baijot, M., and Philippo, S.: Crystal structure of arsenuranospathite from Rabejac, Lodève, France, Eur. J. Mineral., 27, 589–597, https://doi.org/10.1127/ejm/2015/0027-2461, 2015.

Dini, A.: Ore deposits, industrial minerals and geothermal resources, Per. Mineral., 72, 41–52, 2003.

D'Orazio, M., Biagioni, C., Dini, A., and Vezzoni, S.: Thallium-rich pyrite ores from the Apuan Alps, Tuscany, Italy: constraints for their origin and environmental concerns, Miner. Deposita, 52, 687–707, 2017.

Downs, G. W., Yang, B. N., Thompson, R. M., Wenz, M. D., and Andrade, M. B.: Redetermination of durangite, $NaAl(AsO_4)F$, Acta Crystallogr. E, 68, i86–i87, 2012.

Elliott, P., Grey, I. E., and Willis, A. C.: Redefinition of the formula for aldermanite, $[Mg(H_2O)_6][Na(H_2O)_2Al_3(PO_4)_2(OH,F)_6] \cdot H_2O$, and its crystal structure, Mineral. Mag., 85, 348–353, 2021.

Elliott, P., Grey, I. E., MacRae, C. M., Kampf, A. R., and Davidson, C.: Penriceite, $[Mg(H_2O)_6][Na(H_2O)_2Al_3(PO_4)_2F_6] \cdot H_2O$, the F-analogue of aldermanite, from the Penrice marble quarry, South Australia, Australian J. Mineral., 23, 5–12, 2022.

Elliott, P., Grey, I. E., Boer, S., Kampf, A. R., MacRae, C. M., Glenn, A., and Davidson, C.: Chinnerite, $[Mg(H_2O)_6]Na(H_2O)_2Al_3(PO_4)_2F_6$, a new penriceite-related mineral, from the Penrice marble quarry, South Australia, Australian J. Mineral., 25, 5–13, 2024.

Ferraris, G. and Franchini-Angela, M.: Survey of the geometry and environment of water molecules in crystalline hydrates studied by neutron diffraction, Acta Crystallogr. B, 28, 3572–3583, 1972.

Ferraris, G. and Ivaldi, G.: Bond valence vs bond length in O···O hydrogen bonds, Acta Crystallogr. B, 44, 341–344, 1988.

Ferraris, G., Makovicky, E., and Merlino, S.: Crystallography of modular materials, IUCr monographs on Crystallography, 15, Oxford University Press, New York, 382 pp., ISBN 9780199545698, 2008.

Foord, E. E., Oakman, M. R., and Maxwell, C. H.: Durangite from the Black Range, New Mexico, and new data on durangite from Durango and Cornwall, Can. Mineral., 23, 241–246, 1985.

Foord, E. E., Hlava, P. F., Fitzpatrick, J. J., Erd, R. C., and Hinton, R. W.: Maxwellite and squawcreekite, two new minerals from the Black Range tin district, Catron County, New Mexico, U.S.A., Neues Jb. Miner. Monat., 1991, 363–384, 1991.

Foord, E. E., Hughes, J. M., Cureton, F., Maxwell, C. H., Falster, A. U., Sommer, A. J., and Hlava, P. F.: Esperanzaite, $NaCa_2Al_2(As^{5+}O_4)_2F_4(OH) \cdot 2H_2O$, a new mineral species from the La Esperanza mine, Mexico: descriptive mineralogy and atomic arrangement, Can. Mineral., 37, 67–72, 1999.

Fornaseri, M.: Un nuovo ossicloruro di antimonio fra i prodotti di alterazione dell'antimonite alle Cetine di Cotorniano presso Rosia (Siena), Rend. R. Accad. Naz. Lincei, 3, 365–369, 1947.

Goreaud, M. and Raveau, B.: Alunite and crandallite: a structure derived from that of pyrochlore, Am. Mineral., 65, 953–956, 1980.

Grey, I. E., Mumme, W. G., MacRae, C. M., Kampf, A. R., and Mills, S. J.: Elliottite, $NaMgAl_3(PO_4)_2F_6 \cdot 9H_2O$: a new crandallite-derivative mineral from Tom's phosphate quarry, Kapunda, South Australia, Australian J. Mineral., 23, 13–20, 2022.

Holland, T. J. B. and Redfern, S. A. T.: Unit cell refinement from powder diffraction data: the use of regression diagnostics, Mineral. Mag., 61, 65–77, 1997.

Holtstam, D., Bindi, L., Bonazzi, P., Förster, H. J., and Andersson, U. B.: Arrheniusite-(Ce), $CaMg[(Ce_7Y_3)Ca_5](SiO_4)_3(Si_3B_3O_{18})(AsO_4(BO_3)F_{11}$, a new member of the vicanite group, from the Östanmossa mine, Norberg, Sweden, Can. Mineral., 59, 177–189, 2021.

Kraus, W. and Nolze, G.: Powder Cell – a program for the representation and manipulation of crystal structures and calculation of the resulting X-ray powder patterns, J. Appl. Crystallogr., 29, 301–303, 1996.

Lattanzi, P.: Epithermal precious metal deposits of Italy – an overview, Miner. Deposita, 34, 630–638, 1999.

Libowitzky, E.: Correlation of O-H stretching frequencies and O-H···O hydrogen bond lengths in minerals, Monatsh. Chem., 130, 1047–1059, 1999.

Majzlan, J., Drahota, P., and Filippi, M.: Parageneses and crystal chemistry of arsenic minerals, Rev. Mineral. Geochem., 79, 17–184, 2014.

Mandarino, J. A.: The Gladstone-Dale relationship. Part III. Some general applications, Can. Mineral., 17, 71–76, 1979.

Mandarino, J. A.: The Gladstone-Dale relationship. Part IV. The compatibility concept and some application, Can. Mineral., 19, 441–450, 1981.

Maras, A., Parodi, G. C., Della Ventura, G., and Ohnenstetter, D.: Vicanite-(Ce): a new Ca-Th-REE borosilicate from the Vico volcanic district (Latium, Italy), Eur. J. Mineral., 7, 439–446, 1995.

Mauro, D., Biagioni, C., Sejkora, J., Dolníček, Z., and Škoda, R.: Batoniite, $[Al_8(OH)_{14}(H_2O)_{18}](SO_4)_5 \cdot 5H_2O$, a new mineral with the $[Al_8(OH)_{14}(H_2O)_{18}]^{10+}$ polyoxocation from the Cetine di Cotorniano Mine, Tuscany, Italy, Eur. J. Mineral., 35, 703–714, 2023.

Menchetti, S. and Batoni, M.: Le Cetine di Cotorniano. Miniera & Minerali. Associazione Micro-mineralogica Italiana, Cremona, 353 pp., ISBN 978-88-905541-3-1, 2015.

Morteani, G., Voropaev, A., and Grinenko, V.: Relation of stibnite mineralisation and geothermal fluids in southern Tuscany (central Italy): an isotope (C, O, H, S) and Rare Earth Element study, Neues Jb. Miner. Abh., 194, 279–296, 2017.

Olmi, F. and Sabelli, C.: Brizziite, $NaSbO_3$, a new mineral from the Cetine mine (Tuscany, Italy): description and crystal structure, Eur. J. Mineral., 6, 667–672, 1994.

Olmi, F., Sabelli, C., and Trosti-Ferroni, R.: Rosenbergite, $AlF[F_{0.5}(H_2O)_{0.5}]_4 \cdot H_2O$, a new mineral from the Cetine mine (Tuscany, Italy): description and crystal structure, Eur. J. Mineral., 5, 1167–1174, 1993.

Pekov, I. V., Koshlyakova, N. N., Zubkova, N. V., Lykova, I. S., Britvin, S. N., Yapaskurt, V. O., Agakhanov, A. A., Shchipalkina, N. V., Turchkova, A. G., and Sidorov, E. G.: Fumarolic arsenates – a special type of arsenic mineralization, Eur. J. Mineral., 30, 305–322, 2018a.

Pekov, I. V., Zubkova, N. V., Agakhanov, A. A., Yapaskurt, V. O., Chukanov, N. V., Belakovskiy, D. I., Sidorov, E. G., and Pushcharovsky, D. Y.: New arsenate minerals from the Arsenatnaya fumarole, Tolbachik volcano, Kamchatka, Russia. VIII. Arsenowagnerite, $Mg_2(AsO_4)F$, Mineral. Mag., 82, 877–888, 2018b.

Pekov, I. V., Zubkova, N. V., Agakhanov, A. A., Belakovskiy, D. I., Vigasina, M. F., Yapaskurt, V. O., Britvin, S. N., Turchkova, A. G., Sidorov, E. G., and Pushcharovsky, D. Y.: Evseevite, IMA 2019-064, in: CNMNC Newsletter 52, Eur. J. Mineral., 32, https://doi.org/10.5194/ejm-32-1-2020, 2020a.

Pekov, I. V., Britvin, S. N., Yapaskurt, V. O., Koshlyakova, N. N., Polekhovsky, Y. S., Göttlicher, J., Chukanov, N. V., Vigasina, M. F., Krivovichev, S. V., Turchkova, A. G., and Siderov, E. G.: Arsmirandite, $Na_{18}Cu_{12}Fe^{3+}O_8(AsO_4)_8Cl_5$, and lehmannite, $Na_{18}Cu_{12}TiO_8(AsO_4)_8FCl_5$, new minerals from fumarole exhalations of the Tolbachik volcano, Kamchatka, Russia, Zap. Ross. Mineral. Obsh, 149, 1–17, 2020b.

Pekov, I. V., Zubkova, N. V., Agakhanov, A. A., Belakovskiy, D. I., Vigasina, M. F., Britvin, S. N., Turchkova, A. G., Sidorov, E. G., and Pushcharovsky, D. Y.: Polyarsite, IMA 2019-058, in: CNMNC Newsletter 52, Eur. J. Mineral., 32, https://doi.org/10.5194/ejm-32-1-2020, 2020c.

Pekov, I. V., Zubkova, N. V., Agakhanov, A. A., Yapaskurt, V. O., Belakovskiy, D. I., Britvin, S. N., Sidorov, E. G., Kutyrev, A. V., and Pushcharovsky, D. Y.: New arsenate minerals from the Arsenatnaya fumarole, Tolbachik volcano, Kamchatka, Russia. XIX. Axelite, $Na_{14}Cu_7(AsO_4)_8F_2Cl_2$, Mineral. Mag., 87, 109–117, 2023.

Pouchou, J. L. and Pichoir, F.: "PAP" ($\varphi\rho$Z) procedure for improved quantitative microanalysis, in: Microbeam Analysis, edited by: Armstrong, J. T., 104–106, San Francisco Press, San Francisco, 1985.

Roper, A. J., Leverett, P., Murphy, T. D., and Williams, P. A.: The stability of onoratoite, $Sb_8O_{11}Cl_2$, in the supergene environment, Mineral. Mag., 78, 1671–1675, 2014.

Sabelli, C.: I minerali delle Cetine di Cotorniano (SI): i solfati dimorfi jurbanite e rostite, Per. Mineral., 53, 53–65, 1984.

Sabelli, C.: Uklonskovite, $NaMg(SO_4)F \cdot 2H_2O$: new mineralogical data and structure refinement, B. Minéral., 108, 133–138, 1985.

Sabelli, C. and Vezzalini, G.: Cetineite, a new antimony oxide-sulfide mineral from Cetine mine, Tuscany, Italy, Neues Jb. Miner. Monat., 1987, 419–425, 1987.

Sheldrick, G. M.: SHELXT – Integrated space-group and crystal-structure determination, Acta Crystallogr. A, 71, 3–8, 2015a.

Sheldrick, G. M.: Crystal structure refinement with SHELXL, Acta Crystaloogr. C, 71, 3–8, 2015b.

Sillitoe, R. H. and Brogi, A.: Geothermal systems in Northern Apennines, Italy: modern analogues of Carlin-style gold deposits, Econ. Geol., 116, 1491–1501, 2021.

Sjögren, H.: Svabit, ett mineral af apatitgruppen från Harstigsgrfvan, Geol. För. Stockholm Förhand., 13, 789–796, 1891.

Sjögren, H.: Contributions to Swedish mineralogy. Part I: 7. Svabite a new member of the apatite group, Bull. Geol. Inst. Univ. Upsala, 1, 50–56, 1892.

Sjögren, H.: Preliminära meddelanden om några undersökningar på Svenska mineral. 4. Tilasit eller fluor-adelit från Långban, Geol. För. Stockholm Förhand, 17, 291–294, 1895.

Walenta, K.: Uranospathite and arsenuranospathite, Mineral. Mag., 42, 117–128, 1978.

Wedepohl, K. H.: The composition of continental crust, Geochim. Cosmochim. Ac., 59, 1217–1232, 1995.

Wilson, A. J. C. (Ed.): International Tables for Crystallography, Volume C: Mathematical, physical and chemical tables, Kluwer Academic, Dordrecht, NL, 1992.

Wilson, W. E.: Durangite from Utah, Mineral. Rec., 17, 342, 1986.

Wright, F. E.: Computation of the optic axial angle from the three principal refractive indices, Am. Mineral., 36, 543–556, 1951.